Perpendicular electronic transport in doping superlattices

E. F. Schubert, J. E. Cunningham, and W. T. Tsang
AT&T Bell Laboratories, Holmdel, New Jersey 07733

(Received 1 June 1987; accepted for publication 17 July 1987)

Electronic transport measurements are performed at 77 and 300 K on doping superlattices in perpendicular direction to the quantum well planes. The periods of the doping superlattices range from 150 to 600 Å. The current-voltage characteristics in *long period* doping superlattices (type B) are strongly nonlinear and exhibit a new type of negative differential conductivity. The occurrence of negative differential conductivity is caused by avalanche multiplication in the high-field regions of the superlattice and accumulation of holes in the valence-band maxima. In *short period* doping superlattices (type A) the current-voltage characteristics are linear at temperatures of 300 and 77 K showing that tunneling through thin barriers dominates perpendicular transport. The calculation of the tunneling current yields a strong dependence on the period $(\exp - z_p^{3/2})$.

When Esaki and Tsu proposed the famous superlattice concept[1] they did not only consider compositional superlattices, but also doping superlattices. Such doping superlattices can be achieved by alternatingly n- and p-type doping of a semiconductor. The superlattice concept requires, however, that a considerable (i) potential modulation is achieved on a (ii) short length scale. The delta-doping technique[2,3] is well suited to achieve such a considerable modulation on a short length scale, since delta doping allows us to achieve (i) high doping concentrations ($> 10^{13}$ cm^{-2})[4] and a (ii) localization of impurities on a length scale of the lattice constant.[5] These properties of the delta-doping technique made possible the growth and characterization of the Esaki–Tsu type doping superlattice.[6] Hitherto, doping multilayer structures have been restricted to periods of typically 500–1000 Å.[7–9] Periodic semiconductor structures of such a long period are, however, decoupled multiple quantum well structures rather than superlattices in the sense of the original idea by Esaki and Tsu.[1] The physical properties of the present doping superlattices depend strongly on the period length, reflecting a quantum well to superlattice transition.[6] We will therefore refer to short period and long period as type A and type B doping superlattices, respectively.

In this letter we report a new kind of negative differential conductivity (NDC) obtained in type B long period doping superlattices. In short period type A doping superlattices NDC is *not* observed but rather a quite efficient vertical transport due to tunneling through thin barriers. Finally, the tunneling current will be calculated and its dependence on the period will be compared to our experimental findings.

The epitaxial GaAs layers are grown in a modified vacuum generator V80 gas-source molecular beam epitaxy system (GS MBE).[10] The layer sequence of the GaAs samples used in this study is shown schematically in Fig. 1(a). The superlattice consists of alternatingly n-type and p-type delta-doped sheets. The superlattice has ten periods. The two-dimensional doping concentration is $N_A^{2D} = N_D^{2D} = 10^{13}$ cm^{-2}. The superlattices have the periods $z_p = 150$ Å and $z_p = 600$ Å. The parameters are summarized in Table I. The superlattice is grown on an n^+-type substrate. Nonalloyed ohmic contacts are used for contacting the uppermost n-type GaAs layer.[11] Alloyed ohmic contacts were not used to avoid harmful diffusion of impurities into the superlattice. After evaporation of circular Ti/Au (500 Å/2000 Å) contacts (diameter = 250 μm), the GaAs not covered by the contact metal is etched 2.0 μm deep to form mesas as shown in Fig. 1(b). The current-voltage measurements at 77 and 300 K are performed with a Tektronix 576 curve tracer and a Hewlett–Packard 4145A parameter analyzer. Schematic band diagrams of doping superlattices with the same doping concentration but various periods are shown in Fig. 1(c). This figure reveals the sawtooth-shaped potential modulation of magnitude V_z, and the bottom of the lowest subband, E_0. Vertical transport depends sensitively on both barrier thickness and barrier height. The latter one is effectively given by the energy modulation of the superlattice minus the lowest subband energy, i.e., $qV_z - E_0$. These values[3] are listed in Table I, together with the barrier thickness which is $< z_p$. The energy diagram and vertical transport depend strongly on the period of the superlattice. As shown in Fig. 1(c) short period or type A superlattices have thin barriers and small energy modulation. The energy modulation (> 300 meV) is, however, significantly larger than the thermal energy (< 30 meV). As the period increases, carriers are strongly localized within the wells resulting in an array of purely two-dimensional systems. Such type B sawtooth superlattices can be either depleted of free carriers [middle of Fig. 1(c)] or, for even longer periods, nondepleted [bottom of Fig. 1(c)].

The current-voltage (I-V) characteristic at $T = 77$ and

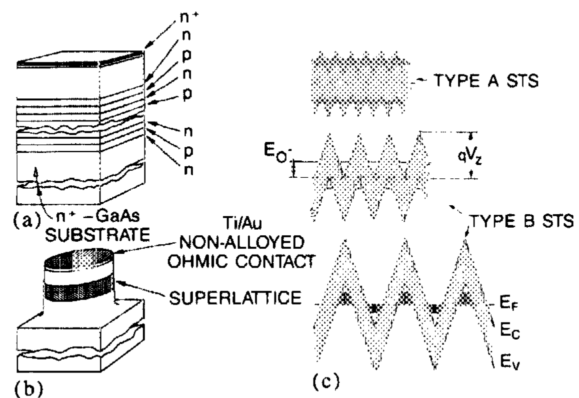

FIG. 1. Schematic sketch of (a) doping superlattice consisting of alternatingly n- and p-type delta-doped layers. (b) Mesa structure used for perpendicular transport measurements. (c) Band diagrams of short-period (type A) and long-period (type B) sawtooth superlattices.

Downloaded 14 Jul 2003 to 128.113.111.105. Redistribution subject to AIP license or copyright, see http://ojps.aip.org/aplo/aplcr.jsp

TABLE I. Design parameters of sawtooth superlattices.

	Type A	Type B
Period length z_p (Å)	150	600
Doping concentration $N^{2D}(cm^{-2})$	1×10^{13}	1×10^{13}
Potential modulation V_z (mV)	518	$>E_g/q$
Electron subband energy E_0 (meV)	188	188

300 K of a short period ($z_p = 150$ Å) sawtooth superlattice is shown in Fig. 2. The I-V curve at 300 K is linear and the total resistance has an areal resistance of $2.3\times10^{-2}\ \Omega\ cm^2$. This resistance is attributed entirely to the superlattice region. Neither the top ohmic contacts nor the Si-doped substrate contributes significantly to the measured I-V characteristic. A linear I-V characteristic is found for the short period doping superlattices also at $T = 77$ K. The total resistance increases at low temperature to 19 Ω yielding an areal resistance of $3.8\times10^{-2}\ \Omega\ cm^2$. At $T = 77$ K, the I-V curve is linear on all scales.

Resonant tunneling (elastic tunneling) occurs if the energy drop per period (also called "Stark ladder energy") is smaller than the miniband width of the superlattice. Thermally assisted (phonon-assisted) sequential tunneling occurs if the Stark ladder energy exceeds the miniband width of the superlattice. The decrease of the perpendicular transport efficiency at low temperature shows, however, that tunneling of carriers through the thin barriers cannot solely account for the vertical transport. In addition, thermionic emission of carriers over the barriers contributes to vertical transport in type A superlattices.

The current-voltage characteristics of a long-period, type B sawtooth superlattice ($z_p = 600$ Å) at the temperatures $T = 300$ and 77 K are shown in Fig. 3. For each temperature the I-V curves are displayed on two scales. Figure 3(a) reveals a strongly blocking, symmetric characteristic at 300 K. Voltages below 1.0 V yield currents in the nA range, indicating the drastically reduced tunneling probability through the thick barriers. Absolute values of voltage exceeding 1.5 V yield, however, an exponentially increasing current. The same qualitative shape is found at liquid-nitrogen temperature, as shown in Fig. 3(c). Comparison of Figs. 3(a) and 3(c) reveals an increased differential resistance at low temperature showing again the relevance of thermally assisted tunneling and thermionic emission for perpendicular carrier transport.

At even larger voltages, a novel type of NDC is observed in the doping superlattice. This double-S-shaped NDC is approximately symmetric with respect to the applied voltage. At room temperature the I-V characteristic shows two NDC regions. The first NDC occurs at small current (-5 mA $< I < +5$ mA) at voltages of 5–7 V. The second NDC region occurs at higher currents above 5 mA. This second NDC regime is observed only at room temperature, but not at $T = 77$ K as the comparison of Figs. 3(b) and 3(d) reveals. The basic symmetric double-S-shaped NDC is, however, also observed at $T = 77$ K. NDC has been found in various other structures.[12-15] None of these structures consists, however, of a superlattice.

The band diagram of a long period sawtooth superlattice is shown in Fig. 4(a). The high barriers of the superlattice are difficult to overcome by thermionic emission. Furthermore, the barriers are thick ($z_p = 600$ Å), yielding an extremely small tunneling probability. Suppressed vertical transport is therefore expected at small deviations from equilibrium, which is indeed measured experimentally. Application of an electric field in the superlattice region causes the superlattice to be tilted homogeneously as shown in Fig. 4(b). Consequently, the barrier height and the barrier width are reduced, which makes possible a small current density. A key characteristic of the superlattice is the high built-in electric fields. If the superlattice is not fully depleted, and electrons as well as holes are present in the ground state (see Fig. 4), the electric field is given by

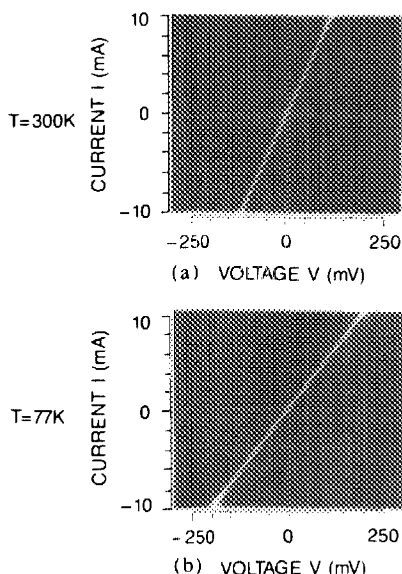

FIG. 2. Current-voltage characteristics of a type A ($z_p = 150$ Å, $N^{2D} = 1\times10^{13}\ cm^{-2}$) sawtooth superlattice at (a) $T = 300$ K and (b) 77 K. The current-density vector is perpendicular on the doping planes.

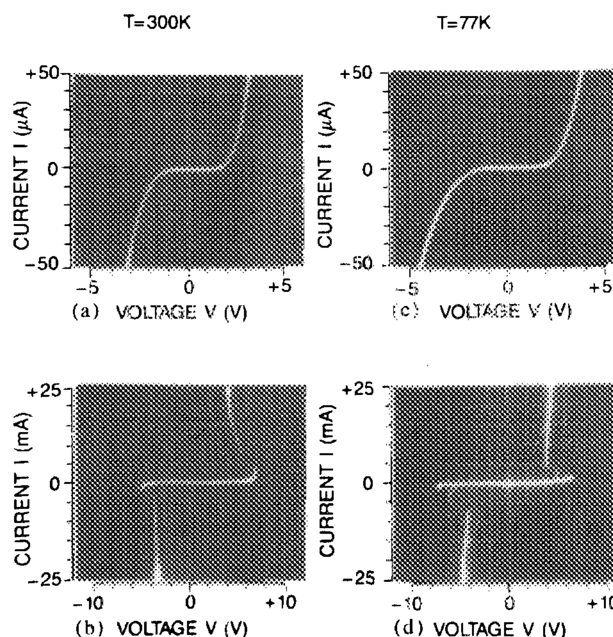

FIG. 3. Current-voltage characteristics of a type B ($z_p = 600$ Å, $N^{2D} = 1\times10^{13}\ cm^{-2}$) sawtooth superlattice at [(a) and (b)] $T = 300$ K and [(c) and (d)] 77 K. The I-V curves are shown on different scales to reveal negative differential conductivity (NDC). The current-density vector is perpendicular to the doping planes.

Downloaded 14 Jul 2003 to 128.113.111.105. Redistribution subject to AIP license or copyright, see http://ojps.aip.org/aplo/aplcr.jsp

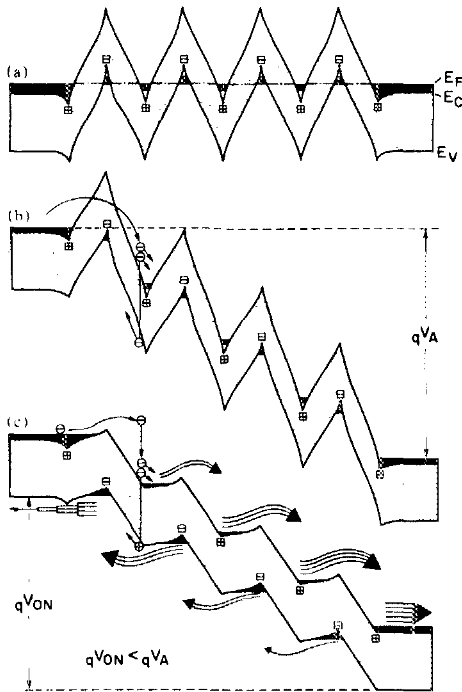

FIG. 4. Schematic sketch of band diagrams of a type B sawtooth superlattice under (a) zero bias, (b) bias causing onset of avalanche effect, and (c) in the negative differential conductivity domain.

$$E = \pm E_g/(qz_p/2) + E_{\text{ext}}, \quad (1)$$

where E_{ext} is the field due to the applied voltage. The electric field E can have a magnitude beyond 5×10^5 V/cm, yielding an avalanche ionization rate of $\alpha \gg 3\times10^4\ \text{cm}^{-1}$. Therefore, at some voltage V_A, avalanche breakdown in one or several periods of the superlattice will occur, as shown in Fig. 4(b). The occurrence of avalanche effect leads to a potential redistribution which manifests itself as negative differential conductivity: Holes, created by avalanche breakdown, will accumulate in the potential maxima of the valence band, due to their heavier effective mass, resulting in a screening of acceptors. The acceptor screening in turn lowers the potential barrier for electron injection into the superlattice region, leading to an increase of the total current density. The redistributed potential is shown in Fig. 4(c) with $V_{\text{on}} < V_A$, i.e., negative differential conductivity.

The interpretation described above is supported by the observation of infrared light emitted from the samples in the NDC domain. Radiative recombination of holes requires generation of holes by the avalanche effect, since there are no holes injected in this (n-type GaAs)-superlattice-(n-type GaAs) structure.

The tunneling probability of an electron with energy E_z through a triangularly shaped barrier of width z_p and height V_z can be obtained from the WKB method according to

$$T(E_z) = \exp\left[-2\frac{\sqrt{2m^*}}{\hbar}\frac{2}{3}\sqrt{qV_z}\,z_p\left(1-\frac{E_z}{qV_z}\right)^{3/2}\right], \quad (2)$$

using $V_z = (1/4)(q/\epsilon)N^{2D}z_p$ yields $j \sim \exp(z_p^\alpha)$ with $\alpha > 3/2$. Such a strong dependence is in excellent agreement with our experimental results.

In conclusion, we have investigated the perpendicular transport properties of type A and type B doping superlattices at $T = 77$ and 300 K by means of current-voltage measurements. Short period doping superlattices exhibit linear I-V characteristics at $T = 77$ and 300 K with a decreasing conductivity at low temperature. Tunneling and thermionic emission dominate perpendicular transport. Long period doping superlattices have completely different nonlinear I-V characteristics, namely, (i) very small tunneling currents at small deviations from equilibrium, (ii) exponentially increasing currents at voltages $1\ \text{V} < V < 5\ \text{V}$, and most interesting (iii) a novel kind of S-type NDC. The NDC is caused by avalanche multiplication in the built-in high-field regions of the superlattice, and a hole accumulation in the valence-band maxima. The resulting screening of acceptor charges enhances the electron injection and gives rise to NDC. The calculation of the tunneling current density yields a strong dependence on the superlattice period: $j \sim \exp(-z_p^\alpha)$ with $\alpha > 3/2$ which corroborates the experimental findings. The study of vertical transport shows unambiguously that type A and type B doping superlattices have very different electronic properties and therefore require individual theoretical approaches.

[1] L. Esaki and R. Tsu, IBM J. Res. Develop. **14**, 61 (1979); for review see L. Esaki, IEEE J. Quantum Electron. **QE-22**, 1611 (1986).
[2] C. E. C. Wood, G. M. Metze, J. D. Berry, and L. F. Eastman, J. Appl. Phys. **51**, 383 (1980).
[3] E. F. Schubert, A. Fischer, Y. Horikoshi, and K. Ploog, Phys. Rev. B **32**, 1085 (1985).
[4] E. F. Schubert, J. E. Cunningham, and W. T. Tsang, Solid State Commun. **63**, 591 (1987).
[5] E. F. Schubert, J. E. Cunningham, W. T. Tsang, and T. H. Chiu (unpublished).
[6] E. F. Schubert, J. E. Cunningham, and W. T. Tsang, Phys. Rev. B **36**, 1348 (1987).
[7] B. A. Vojak, G. W. Zajac, F. A. Chambers, J. M. Meese, P. E. Chumbley, R. W. Kaliski, N. Holonyak, Jr., and D. W. Nam, Appl. Phys. Lett. **48**, 251 (1986).
[8] K. Ploog and G. H. Dohler, Adv. Phys. **32**, 285 (1983).
[9] G. H. Dohler, Phys. Status Solidi B **52**, 533 (1972); **52**, 79 (1972); for a review see IEEE J. Quantum Electron. **QE-22**, 1682 (1986).
[10] J. E. Cunningham, T. H. Chiu, A. Ourmazd, J. Shah, and W. T. Tsang, J. Appl. Phys. **60**, 4165 (1986).
[11] E. F. Schubert, J. E. Cunningham, W. T. Tsang, and T. H. Chiu, Appl. Phys. Lett. **49**, 292 (1986).
[12] G. W. Taylor, J. G. Simmons, A. Y. Cho, and R. S. Mand, J. Appl. Phys. **59**, 596 (1986).
[13] A. E. Owen and J. M. Robertson, IEEE Trans. Electron Devices **ED-20**, 105 (1973).
[14] T. Yamamoto and M. Morimoto, Appl. Phys. Lett. **20**, 269 (1972).
[15] C. E. C. Wood, L. F. Eastman, K. Board, K. Singer, and R. Malik, Electron. Lett. **18**, 676 (1982).

Downloaded 14 Jul 2003 to 128.113.111.105. Redistribution subject to AIP license or copyright, see http://ojps.aip.org/aplo/aplcr.jsp